Reconstruction of firing rate changes across neuronal populations by temporally deconvolved Ca^{2+} imaging

Emre Yaksi & Rainer W Friedrich

Methods to record action potential (AP) firing in many individual neurons are essential to unravel the function of complex neuronal circuits in the brain. A promising approach is bolus loading of Ca^{2+} indicators combined with multiphoton microscopy. Currently, however, this technique lacks cell-type specificity, has low temporal resolution and cannot resolve complex temporal firing patterns. Here we present simple solutions to these problems. We identified neuron types by colocalizing Ca^{2+} signals of a red-fluorescing indicator with genetically encoded markers. We reconstructed firing rate changes from Ca^{2+} signals by temporal deconvolution. This technique is efficient, dramatically enhances temporal resolution, facilitates data interpretation and permits analysis of odor-response patterns across thousands of neurons in the zebrafish olfactory bulb. Hence, temporally deconvolved Ca^{2+} imaging (TDCa imaging) resolves limitations of current optical recording techniques and is likely to be widely applicable because of its simplicity, robustness and generic principle.

The simultaneous recording of AP firing from many individual neurons in the intact brain is one of the fundamental technical challenges in neuroscience. Microelectrode measurements are highly informative but the number of simultaneous recordings is limited by technical constraints. *In vivo* imaging approaches are promising alternatives, but most methods cannot resolve individual neurons and have low temporal resolution[1–3]. Recently, however, Ca^{2+} signals from hundreds of individual neurons were measured by multiphoton microscopy[4,5] after loading of fluorescent Ca^{2+} indicators by bolus injection[6,7] of acetoxymethyl esters[6–11]. Nevertheless, this approach still has two major limitations. First, different neuron types cannot be distinguished because the indicator is loaded nonspecifically. Second, the ability to resolve complex temporal changes in AP firing is severely limited because Ca^{2+} transients are much slower than APs.

APs open voltage-gated Ca^{2+} channels and produce unitary Ca^{2+} transients with a fast rise and a stereotyped, usually exponential, decay[12]. During trains of APs, individual transients summate and generate complex temporal variations in Ca^{2+} concentration. Assuming that AP-related Ca^{2+} transients account for most of the intracellular Ca^{2+} variations, these variations can be approximated by a convolution of the AP train with the waveform of the unitary Ca^{2+} transient. We therefore reasoned that changes in AP firing rate may be reconstructed from the somatic Ca^{2+} signal by the inverse process, that is, a deconvolution (**Supplementary Fig. 1** online).

We tested this approach using the olfactory bulb of adult zebrafish as an experimental model. The olfactory bulb receives afferent input from sensory neurons and contains principal glutamatergic neurons, the mitral cells and local interneurons, the periglomerular and granule cells. Interneurons are numerous and predominantly GABAergic. Mitral cells and interneurons form a reciprocally connected network that processes sensory input and produces temporally patterned olfactory bulb output activity[13,14]. Different types of olfactory bulb neurons can be identified in transgenic zebrafish lines expressing fluorescent proteins[9,15,16]. Experiments were performed in an explant of the intact zebrafish brain and nose that permits simultaneous optical and electrophysiological recordings of odor responses in the olfactory bulb[17].

Our results demonstrate that firing rate changes in populations of individual neurons can be reconstructed efficiently by TDCa imaging. Moreover, we could identify neuron types by spectral separation of Ca^{2+} signals and genetically encoded cell-type markers. We used TDCa imaging to analyze odor-evoked, spatiotemporal activity patterns across thousands of neurons.

RESULTS

Imaging of Ca^{2+} signals and fluorescent cell-type markers

Cell types may be identified by colocalizing Ca^{2+} signals with genetically encoded fluorescent markers. But the emission spectra of commonly used Ca^{2+} indicators overlap extensively with those of green or yellow fluorescent proteins. We therefore examined whether Ca^{2+} signals from populations of neurons can be recorded with any of the red-fluorescing indicators Calcium Orange, Calcium Crimson, Fura Red or rhod-2.

Bolus loading[6,7] of cell-permeable rhod-2–acetoxymethyl ester (rhod-2–AM), but not of the other cell-permeable indicators, resulted in cytoplasmic fluorescence after cleavage of the acetoxymethyl ester by intracellular esterases (**Fig. 1**) that remained high for >8 h. Dye uptake occurred in a volume up to 300 μm in diameter with very little cell damage, as determined by coinjection of a marker for necrotic cell death (**Supplementary Methods**

Max Planck Institute for Medical Research, Department of Biomedical Optics, Jahnstr. 29, 69120 Heidelberg, Germany. Correspondence should be addressed to R.F. (rainer.friedrich@mpimf-heidelberg.mpg.de).

RECEIVED 12 DECEMBER 2005; ACCEPTED 20 MARCH 2006; PUBLISHED ONLINE 20 APRIL 2006; DOI:10.1038/NMETH874

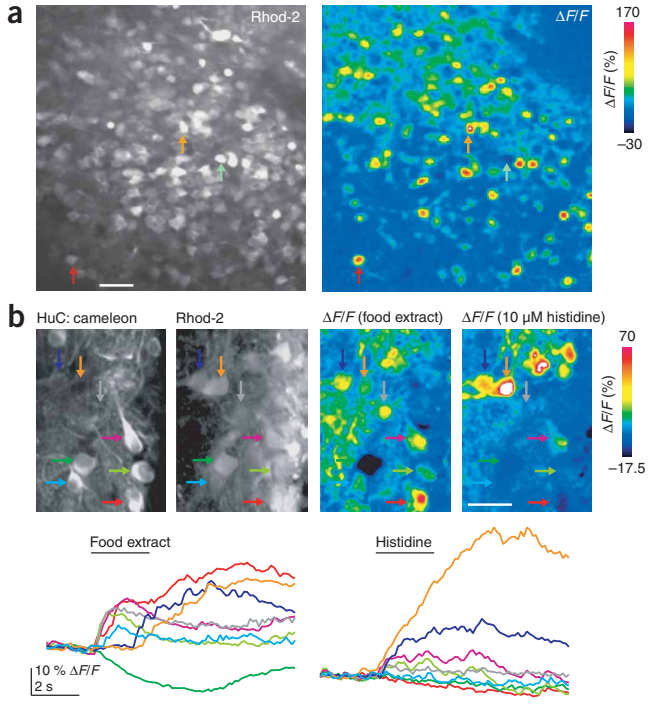

Figure 1 | Two-photon imaging of neuronal calcium signals in the zebrafish olfactory bulb. (**a**) Rhod-2 fluorescence (left) and time-averaged relative change in fluorescence intensity ($\Delta F/F$; right) evoked by odor stimulation (food extract) in the granule cell layer. Scale bar, 25 μm. (**b**) Colocalization of transgenic mitral cell marker (HuC:cameleon; yellow emission channel), rhod-2 labeling (red emission channel) and time-averaged change in rhod-2 fluorescence evoked by two odors (top). Arrows mark eight individual somata. Traces show temporal response patterns (bottom); trace colors correspond to arrows.

online). After loading of rhod-2, odor stimulation evoked spatiotemporal patterns of Ca^{2+} signals in the olfactory bulb (**Fig. 1**) that were large, reproducible, stable over hours and odor-dependent. In transgenic zebrafish (HuC:cameleon) expressing the yellow fluorescent protein (yellow cameleon 2.1; cameleon), in mitral cells[9,16], somatic Ca^{2+} signals from individual mitral cells could clearly be identified by the colocalization of cameleon (**Fig. 1b**). Hence, multiphoton Ca^{2+} imaging using rhod-2 permits the identification of neuron types in animals expressing green- or yellow-fluorescent cell-type markers.

Simultaneous recording of neuronal Ca^{2+} signals and APs

We then compared the intermediate-affinity indicator, rhod-2 (K_D = 570 nM), to the commonly used green-fluorescent high-affinity indicator, Oregon Green 488 BAPTA-1 (OGB-1; K_D = 170 nM). We loaded both indicators simultaneously, measured somatic fluorescence in separate emission channels and recorded APs of individual neurons with a micropipette (n = 28 neurons). In experiments using odor stimulation, APs were usually recorded in the loose-patch configuration. To control AP firing more directly by current injection, we performed recordings in the juxtacellular mode[18]. Using this technique the plasma membrane is punctured to permit current access, but this causes a gradual washout of Ca^{2+} signals. Peak firing rates evoked by odor stimulation transiently reached ~100 Hz in mitral cells but rarely exceeded 25 Hz in interneurons.

Individual APs or brief bursts were associated with discrete somatic Ca^{2+} signals in mitral cells and interneurons (**Fig. 2a**). Scaled Ca^{2+} signals measured with rhod-2 and OGB-1 were similar. The decay of Ca^{2+} transients could be fitted by single exponentials with a time constant of $\tau = 3.8 \pm 2.4$ s in mitral cells (mean ± s.d.; n = 24) and $\tau = 5.7 \pm 2.3$ s in interneurons (n = 19; $P < 0.01$; **Supplementary Fig. 2** online). During trains of bursts, Ca^{2+} signals summed extensively (**Fig. 2a**). To examine saturation of Ca^{2+}

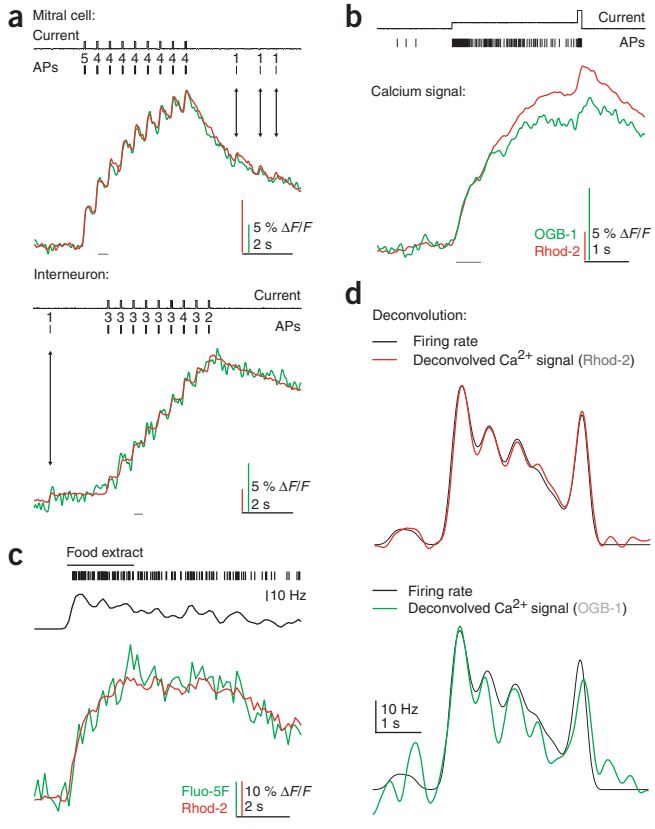

Figure 2 | Relationship between APs and Ca^{2+} signals. (**a**) Simultaneous recording of APs, changes in rhod-2 fluorescence (red) and changes in OGB-1 fluorescence (green) in a mitral cell and an interneuron. Bursts of APs were evoked by brief current injections. Numbers indicate number of APs per burst. Arrows depict single spontaneous APs and associated Ca^{2+} transients. Traces were scaled by normalizing to the average $\Delta F/F$ value during the periods indicated by gray bars. Mitral cell was hyperpolarized to decrease spontaneous firing. Images were acquired at 32 ms/frame. (**b**) Simultaneous recording of APs, changes in rhod-2 fluorescence (red) and changes in OGB-1 fluorescence (green) in a mitral cell. Sustained high-frequency firing was evoked by current injection (top trace) for 3 s. At the end, a terminal burst was evoked by an additional current step. Traces were scaled by normalizing to the $\Delta F/F$ signal during the period indicated by the gray bar. (**c**) Simultaneous recording of odor-evoked AP firing (ticks), change in rhod-2 fluorescence (red), and change in Fluo-5F fluorescence (green) in a mitral cell. Black trace shows firing rate, obtained by convolution of the spike train with a Gaussian (σ = 128 ms). (**d**) Firing rate (black; σ = 128 ms) and deconvolved Ca^{2+} signals of the data in **b** (after filtering). Time scale aligned to **b**. τ_{decay} for deconvolution (4.1 s) was determined by measuring the decay time constant of calcium transients in the same mitral cell.

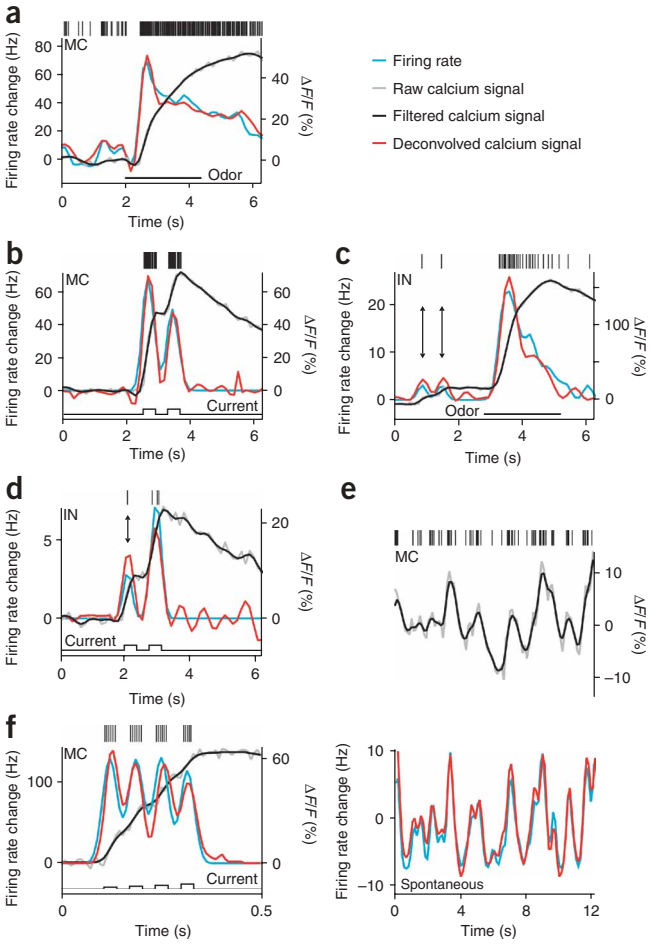

Figure 3 | Temporal deconvolution of two-photon Ca^{2+} signals. (**a**–**f**) Each panel shows firing rate changes and simultaneously recorded Ca^{2+} signals before filtering, after filtering, and after filtering and deconvolution in an individual neuron. Firing rate traces are spike trains (ticks) convolved with a Gaussian. Frame duration and σ of the Gaussian were 128 ms unless noted otherwise. Ca^{2+} signals were filtered and deconvolved using $\tau_{decay} = 3$ s, $thr_{noise} = 1\%$ for mitral cells and $\tau_{decay} = 6$ s, $thr_{noise} = 1\%$ for interneurons unless noted otherwise. Mitral cell (MC) odor response (**a**). Mitral cell response to two current pulses; spontaneous firing was prevented by hyperpolarizing current (**b**). Interneuron (IN) odor response; arrows mark individual APs and associated Ca^{2+} transients (**c**). Interneuron response to two brief, low-intensity current injections; arrow marks an individual AP and associated Ca^{2+} transient (**d**). Spontaneous mitral cell firing; traces showing raw and deconvolved Ca^{2+} signals are separated for clarity (**e**). Mitral cell response to four brief current pulses with duration and interval of 32 ms, imaged at high temporal resolution (8 ms/frame; **f**). Spikes were convolved with a Gaussian with $\sigma = 15$ ms; Ca^{2+} signals were Gaussian filtered with the same σ. Increasing current amplitudes were used to evoke approximately equal numbers of APs during each pulse.

signals, we evoked sustained firing by continuous current injection or by odor stimulation. Scaled somatic Ca^{2+} signals were initially similar but the rhod-2 signal eventually exceeded the OGB-1 signal (**Fig. 2b**), indicating that OGB-1 signal, but not rhod-2 signal, approached saturation. When we loaded rhod-2 together with the low-affinity Ca^{2+} indicator, fluo-5F ($K_D = 2.3$ μM; $n = 17$ neurons), scaled somatic Ca^{2+} signals did not deviate during sustained firing (**Fig. 2c**). These results indicate that rhod-2 is well suited for multiphoton Ca^{2+} imaging of neuronal activity and exhibits little or no saturation during physiological patterns of AP firing.

Reconstruction of firing rate changes from Ca^{2+} signals

We then explored whether dynamic patterns of firing rate changes can be reconstructed from somatic Ca^{2+} signals by deconvolution. Before deconvolution, we attenuated small fluctuations in the Ca^{2+} signal, most likely shot noise, by two filtering procedures. First, Ca^{2+} signals were smoothed using a low-pass Butterworth or Gaussian filter. Subsequently, Ca^{2+} signals were further filtered using an empirically designed procedure that smoothes peaks with amplitudes below a threshold, thr_{noise}, by local averaging (**Supplementary Fig. 3** online). These filtering procedures effectively removed low-amplitude fluctuations with minimal distortions of fast Ca^{2+} transients. Filtered somatic Ca^{2+} signals were then deconvolved with an exponentially decaying kernel. When the kernel time constant, τ_{decay}, was determined from Ca^{2+} transients in the same neuron, time-varying firing rate changes could be reconstructed accurately from the rhod-2 signal, and elevated firing rates could be followed for several seconds (**Fig. 2d** and **Supplementary Fig. 2**). Reconstruction based on the OGB-1 signal began to deviate from the real firing rate change when the indicator approached saturation (**Fig. 2d**). Hence, complex temporal activity patterns can be reconstructed from the rhod-2 signal by deconvolution.

Decay time constants may vary somewhat between neurons of the same type as a result of differences in biophysical properties and in intracellular indicator concentration (**Supplementary Fig. 2**). When firing rate patterns are to be reconstructed from large populations it becomes impossible to determine these time constants for each individual neuron. We therefore examined reconstruction efficiency when τ_{decay} was fixed to 3 s for mitral cells and 6 s for interneurons. We derived these values from measurements of decay time constants (**Supplementary Fig. 2**) and from a parameter search (see below). AP firing was modulated in individual neurons by odor stimulation and current injection to create a wide variety of firing patterns, including long-lasting high-frequency firing (**Fig. 3a**), abrupt transitions in firing rate (**Fig. 3b**), decreasing firing rates (**Fig. 3c**) and sparse APs (**Fig. 3d**). In all cases, the raw Ca^{2+} signal differed substantially from the temporal firing pattern, but the temporally deconvolved Ca^{2+} signal closely followed the actual firing rate change. Hence, firing rate reconstruction was efficient even when τ_{decay} was not determined individually for each neuron (see also **Supplementary Fig. 2**).

We also explored whether TDCa imaging can reveal small firing rate changes around a low mean. In mitral cells, spontaneous firing rate fluctuations around a mean rate of 5–10 Hz were reconstructed accurately by TDCa imaging (**Fig. 3e**). Interneurons fired sparse APs at a rate of <1 Hz. Most of such isolated APs were associated with a distinct Ca^{2+} transient and could be identified in the deconvolved signal (**Fig. 3c**,**d**). We occasionally observed Ca^{2+} transients not associated with AP firing in interneurons, particularly during periods after elevated AP firing (see **Fig. 3d** for a prominent example). These events were small, however, even in comparison to Ca^{2+} transients evoked by single APs (**Fig. 3c**,**d**). Out of 56 individual APs that were separated from other APs by at least 256 ms, 50 were detected by simple thresholding of the deconvolved Ca^{2+} signal, with two false positives. Therefore,

Table 1 | Reconstruction efficiency as a function of τ_{decay} and thr_{noise}

Data set	τ_{decay} (s; range)	thr_{noise} (percent $\Delta F/F$; range)	Reconstruction efficiency (range)
1	1–6	0–3	0.78–0.87
2	1–5	0–3	0.88–0.91
3	3–10	0–3	0.87–0.90

For both parameters, reconstruction efficiency was high throughout a considerable range.

individual APs in interneurons were detected with a success rate of 86%. Moreover, bursts of APs could often be distinguished from individual APs based on the amplitude of the deconvolved Ca^{2+} signal (**Fig. 3d**).

We determined the maximum temporal resolution of TDCa imaging by injecting current steps with durations and interpulse intervals of 100, 50, 32 or 16 ms into mitral cells ($n = 2$–4 mitral cells for each setting) while acquiring images at 8 ms/frame. The deconvolved Ca^{2+} signal followed the evoked AP bursts down to 32-ms intervals (**Fig. 3f**) but only partially followed patterns with 16 ms intervals (data not shown). Hence, TDCa imaging can separate bursts of APs with a temporal resolution of ~30 ms.

Quantitative analysis of reconstruction efficiency

We quantified the reliability of reconstructing firing rate changes by TDCa imaging in three data sets containing simultaneous records of APs and Ca^{2+} signals from multiple neurons. Data set 1 comprised 49 odor responses of 8 mitral cells recorded in the loose-patch configuration. Data set 2 contained 21 responses, each from a different mitral cell, evoked by temporally patterned current injection. Data set 3 contained 16 responses of different interneurons to odor stimulation or current injection. Neurons in data sets 2 and 3 were recorded in the juxtacellular configuration.

Our deconvolution procedure requires the specification of two parameters: the decay time constant of the exponential kernel, τ_{decay}, and the threshold for the filtering procedure, thr_{noise}. We varied both parameters over a wide range and determined the correlation coefficient between the measured and reconstructed firing rate pattern of each neuron. We then quantified reconstruction efficiency by the average correlation coefficient in each data set as a function of τ_{decay} and thr_{noise}. Maximum reconstruction efficiencies were 0.87, 0.91 and 0.90 for data sets 1–3, using values for τ_{decay} and thr_{noise} of 3 s and 0.2%, 2 s and 0.2%, and 7 s and 2%, respectively. The fraction of the variance recovered was 77%, 84% and 81%, respectively. Notably, reconstruction efficiency was high throughout a wide range of both parameters (**Table 1** and **Supplementary Fig. 4** online). This demonstrates that the reconstruction procedure is robust even if optimal parameter values are not determined precisely by electrophysiology studies.

Temporal patterns of deconvolved Ca^{2+} signals, but not patterns of raw Ca^{2+} signals, closely resembled the simultaneously measured patterns of firing rate changes in each response (**Fig. 4a–c**). Moreover, the relationship between real and reconstructed firing rate changes was linear over the full range of firing rate changes observed in all three data sets (**Fig. 4d–f**) indicating that potential nonlinearities in the relationship between firing rate changes and Ca^{2+} signals (for example, dye saturation) did not noticeably distort the reconstruction. Hence, the diverse temporal patterns of firing rate changes contained in the three data sets were reconstructed efficiently by TDCa imaging.

Measurement of the patterns of firing rate changes across populations not only requires the correct reconstruction of temporal response patterns in individual neurons, but also of relative response amplitudes across neurons. We therefore combined responses from all individual neurons in each data set into a single pattern without individual scaling of trials. These combined patterns represent population activity as it would be recorded in experiments without simultaneous electrophysiological information available. Reconstructed population activity patterns were very similar to the original patterns of firing rate changes, and to reconstructions of firing rate patterns when each trial was scaled individually (**Fig. 4a–c**). In data set 1, the reconstruction efficiency for population activity was 0.86 and the fraction of variance recovered was 74%. This is almost identical to the reconstruction efficiency for single neuron responses. For data sets two and three, reconstruction efficiency for population activity patterns was slightly lower (0.80 and 0.77, respectively), which is, however, at least partially due to washout effects associated with juxtacellular recordings. Hence, TDCa imaging can also be used to efficiently reconstruct spatiotemporal patterns of firing rate changes across neuronal populations.

Odor-evoked activity patterns in the zebrafish olfactory bulb

We used TDCa imaging to measure activity patterns in the olfactory bulb evoked by 16 amino acid odors (10 μM). We

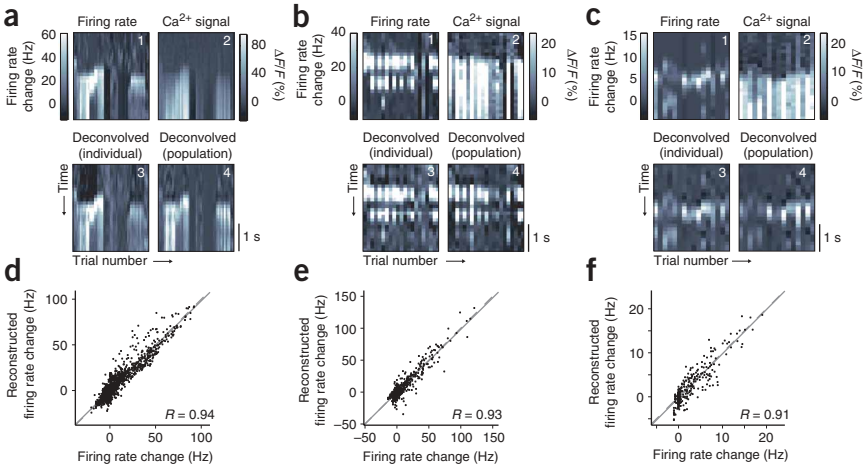

Figure 4 | Quantitative analysis of TDCa imaging. (**a**) Display of all responses in data set 1 as a spatiotemporal pattern. 1, firing rate change; 2, raw Ca^{2+} signal; 3, deconvolved Ca^{2+} signal, scaled individually for each trial; 4, deconvolved Ca^{2+} signal, scaled with the same factor for the whole population. (**b**,**c**) Display of all responses in data sets 2 (**b**) and 3 (**c**) as in **a**. (**d**–**f**) Plot of reconstructed firing rate change against real firing rate change including all trials and time points in each data set. Solid lines, linear fit; dashed lines, line with slope 1.

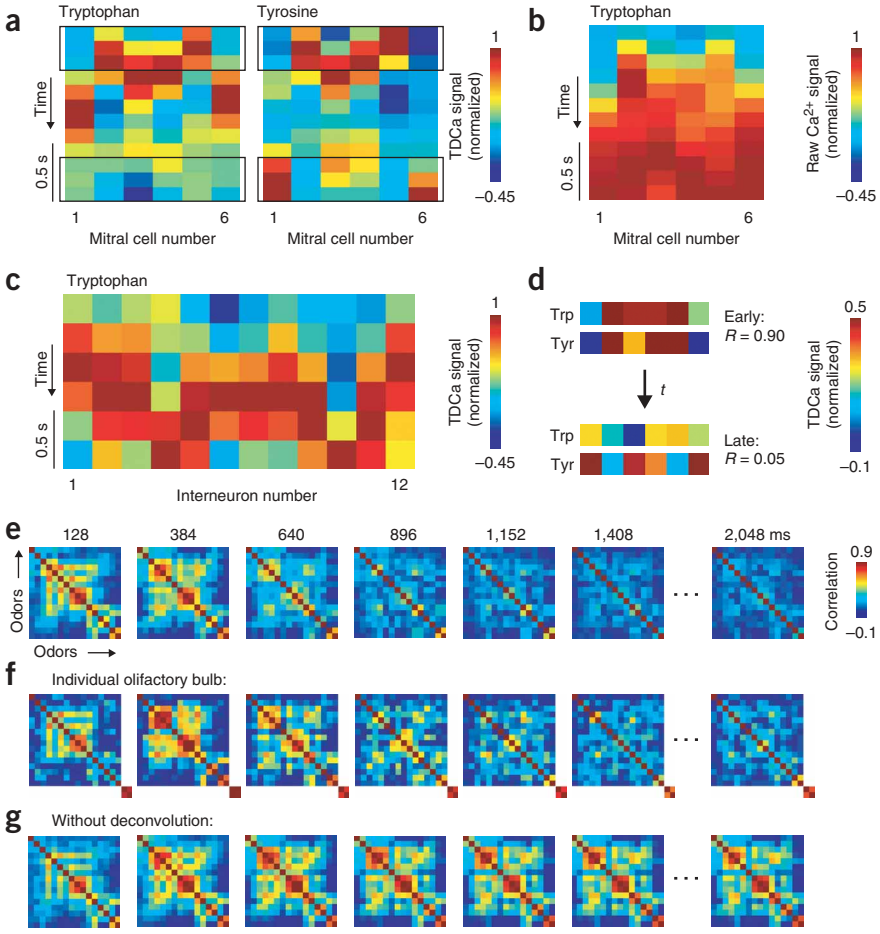

Figure 5 | Analysis of odor-evoked activity patterns in the zebrafish olfactory bulb. (**a**) TDCa signal as a function of time, evoked by two chemically similar amino acids in six mitral cells. Signals were normalized to the maximum signal in each column. (**b**) Raw Ca^{2+} signal evoked by tryptophan as a function of time. Each column normalized to the maximum. (**c**) TDCa signal evoked by tryptophan across 12 interneurons in another olfactory bulb. (**d**) Comparison of activity patterns evoked by tyrosine and tryptophan across the 6 mitral cells in **a**, averaged during the first and last three time bins (boxes in **a**). (**e**) Color-coded correlation matrices depicting the pairwise similarities between TDCa signal patterns evoked by different odors across mitral cells in successive 256-ms time windows. Clusters of high correlation coefficients indicate that groups of related odors evoked similar activity patterns. Data from 1,313 mitral cells in 9 olfactory bulbs. Order of stimuli on both axes is Glu, Asp, Gly, Ala, Ser, His, Asn, Phe, Tyr, Trp, Leu, Met, Val, Ile, Arg and Lys. (**f**) Correlation between TDCa signal patterns across 161 mitral cells in a single olfactory bulb, evoked by the same stimuli as in **e**. In addition, pixels in the lower right show correlation between patterns evoked by two repeated applications of the same stimulus (amino acid mixture). (**g**) Correlations between patterns of Ca^{2+} signals without deconvolution. Same data set as in **e**.

identified mitral cells using the transgenic line, HuC:cameleon (**Fig. 1b**). We applied each stimulus repeatedly while measuring responses at different focal planes in the lateral and central olfactory bulb containing most amino acid–responsive neurons[17,19]. Raw Ca^{2+} signals were deconvolved using parameters within the optimal range for each cell type (mitral cells: $\tau_{decay} = 3$ s, $thr_{noise} = 1\%$; interneurons: $\tau_{decay} = 6$ s, $thr_{noise} = 1\%$). In total, we analyzed responses from 1,313 mitral cells ($n = 9$ olfactory bulbs; 146 ± 45 mitral cells per olfactory bulb; mean $\pm$ s.d.) and 8,009 interneurons ($n = 4$ olfactory bulbs; 2002 ± 611 interneurons per olfactory bulb). Responses from a much smaller set of mitral cells to the same stimuli had been recorded previously by electrophysiology studies[17,20,21]. Odor response patterns of interneurons, in contrast, have not been studied extensively.

TDCa imaging showed that mitral cell responses were highest shortly after stimulus onset and temporally modulated in a stimulus-dependent manner (**Fig. 5a**), consistent with electrophysiological results[17,20]. Without temporal deconvolution, the dynamics of mitral cell activity patterns was not resolved accurately (**Fig. 5b**). Interneuron responses increased more gradually, reached their maxima usually at later times, and also changed during the initial phase of an odor response (**Fig. 5c**).

Electrophysiological studies in zebrafish reported that mitral cell activity patterns evoked by chemically related odors are initially similar but become progressively more dissimilar during the first few hundred milliseconds of an odor response[17,20,21]. This decorrelation enhances pattern discriminability by reducing redundancy and amplifying differences. Previous studies, however, were based on a limited number of mitral cell recordings from different animals. We therefore reexamined pattern decorrelation by TDCa imaging. We first examined responses of mitral cells in the same olfactory bulb to chemically related odor stimuli (**Fig. 5a**). Shortly after response onset, activity patterns across small groups of mitral cells were often similar and highly correlated. Subsequently, however, each activity pattern changed in a different, stimulus-specific fashion. As a consequence, patterns became decorrelated and more distinct (**Fig. 5d**).

We then quantified the similarity of activity patterns evoked by the 16 amino acids across all 1,313 mitral cells by their correlation coefficients in successive time windows (length, 256 ms). Shortly after stimulus onset, mitral cell activity patterns evoked by groups of chemically related stimuli were similar, as shown by clusters of high correlation coefficients along the diagonal of the correlation matrix (**Fig. 5e**). Subsequently, high-correlation coefficients disappeared, indicating that initially similar activity patterns became more distinct. We observed this pattern decorrelation in each individual olfactory bulb (**Fig. 5f**). Correlations between activity patterns evoked by repeated applications of the same stimulus decreased only sightly (**Fig. 5f**). These results are consistent with previous electrophysiological data and confirm that the decorrelation of mitral cell activity patterns is not an artifact of pooling responses from different animals. Without deconvolution, the decorrelation of mitral cell activity patterns cannot be detected in Ca^{2+} imaging data (**Fig. 5g**), demonstrating that the reconstruction

of time-varying firing rate patterns is necessary to observe this computation.

DISCUSSION

Our results demonstrate that neuronal firing rate changes of many individual neurons can be reconstructed efficiently and robustly by TDCa imaging. Moreover, common transgenic fluorescent markers can be used to identify neuron types underlying Ca^{2+} signals measured with the red-fluorescing indicator, rhod-2. Cell type-selectivity is a potential advantage of genetically encoded Ca^{2+} indicators[22] but synthetic Ca^{2+} indicators provide a higher signal-to-noise ratio and faster kinetics. Our approach combines the advantages of synthetic Ca^{2+} indicators and transgenic cell-type labeling, and exploits the existing repertoire of transgenic animals. Moreover, rhod-2 is well suited for neuronal activity measurements because of its intermediate affinity, broad dynamic range and low noise.

Individual APs or discrete bursts have previously been identified from Ca^{2+} signals by approaches designed to detect temporally sparse events, such as spontaneous activity in brain slices[23] or under anaesthesia[11]. These techniques are, however, not suitable to reconstruct AP firing when Ca^{2+} transients overlap significantly (**Supplementary Fig. 5** online). Assuming a decay time constant of $\sim$1 s in the mammalian brain[11], detection of AP firing would be limited to event rates $<$1 Hz. In many brain areas and species, however, AP firing exceeds this frequency limit and can display complex temporal patterns[24–27]. Unlike other techniques, TDCa imaging can be used to reconstruct such firing patterns because it is based on the generic relationship between APs and Ca^{2+} transients (**Supplementary Fig. 1**). TDCa imaging therefore overcomes limitations of previous techniques and is expected to be useful for a wide range of applications.

The efficiency of TDCa imaging may be ultimately limited by shot noise. However, we were able to achieve tolerable noise levels in many cases by standard low-pass filtering of Ca^{2+} signals. In addition, we developed a simple procedure based on local averaging that further reduced noise without noticeable distortions of the reconstructed signal. The detection of Ca^{2+} signals at the soma may be advantageous because synaptic Ca^{2+} transients originating in the dendrites are attenuated, and because somatic Ca^{2+} signals should reach saturation later than dendritic signals.

Our deconvolution procedure requires two parameters, τ_{decay} and thr_{noise}, that may be optimized for each cell type by simultaneous electrophysiological recordings. Reconstruction efficiency, however, was stable within a wide range of both parameters, implying that it is high even when optimal parameters are not determined precisely. It should thus be sufficient for many applications to estimate parameters without simultaneous electrophysiology studies. Simple estimates of τ_{decay} and thr_{noise} can be obtained from the decay of spontaneous Ca^{2+} transients and from the noise of filtered Ca^{2+} signals, respectively.

The maximal temporal resolution ($\sim$30 ms in mitral cells) demonstrates that deconvolution can increase the effective temporal resolution of Ca^{2+}-based activity measurements by a factor of $\sim$100 compared to the τ_{decay} of raw Ca^{2+} signals. A further increase in temporal resolution should be achievable by hardware modifications improving the signal-to-noise ratio. Temporal resolution should also be higher in neurons with faster τ_{decay}, such as mammalian neurons at physiological temperature[11]. It thus remains to be determined whether TDCa imaging will be able to resolve the synchronization of APs in neuronal ensembles with a precision of a few milliseconds[13,28].

The greatest potential of TDCa imaging may be measurements of spatiotemporal activity patterns across large populations of neurons. The fraction of variance recovered from odor-evoked firing patterns across mitral cells recorded in the loose-patch configuration (74%) may be taken as a conservative measure of reconstruction quality. The reliability of population activity measurements is further confirmed by the close correspondence between previous electrophysiological analyses of odor-evoked mitral cell firing patterns[17,20] and the results obtained by TDCa imaging. Another advantage of TDCa imaging is that it permits the detailed geometrical reconstruction of neuronal activity patterns.

TDCa imaging of population odor responses in the olfactory bulb confirmed that initially similar mitral cell activity patterns decorrelate over time. Without temporal deconvolution, correlations between patterns of odor-evoked Ca^{2+} signals across mitral cells remained high and resembled correlations between glomerular input patterns[19], presumably because pattern changes are masked by Ca^{2+} signals generated during the initial phase of the odor response. In insects, Ca^{2+} imaging results have suggested that patterns of glomerular input activity are similar to patterns of output neuron activity[29,30], whereas electrophysiological results indicate that input and output activity patterns diverge over time[27]. Our data suggest that this apparent discrepancy may, at least partially, result from the masking of pattern dynamics by initial Ca^{2+} transients when Ca^{2+} signals are not deconvolved. This consideration illustrates the importance of reconstructing firing rate changes from Ca^{2+} signals. Further promising applications of TDCa imaging in the olfactory system include the possibility to measure response patterns across large numbers of interneurons.

METHODS

Electrophysiology and imaging. We performed experiments in an explant of the intact brain and nose from adult zebrafish[17]. We performed loose-patch extracellular recordings as described previously[17]. We performed juxtacellular recordings[18] in a similar fashion but the recording pipette contained intracellular solution and the plasma membrane was partially disrupted to permit current injection. We dissolved acetoxymethyl esters of Ca^{2+} indicators (50 μg) in 16 μl DMSO/Pluronic F-127 (80/20), diluted them 1:10 in artificial cerebrospinal fluid and pressure-injected them into the olfactory bulb. We delivered amino acid odors (10 μM) and performed two-photon imaging (excitation wavelength, 830 nm) as described previously[9]. We acquired images at 128 ms/frame unless noted otherwise. All animal procedures were performed in accordance with the animal care guidelines issued by the Federal Republic of Germany. See **Supplementary Methods** for further information on animals, electrophysiology, dye injection and imaging procedures.

Filtering and deconvolution. We converted the measured fluorescence intensities to relative changes in fluorescence intensity ($\Delta F/F$) in each pixel and frame. We determined the baseline fluorescence intensity, F, by averaging of frames before stimulus onset. We temporally filtered $\Delta F/F$ signals from individual somata by a low-pass Butterworth or Gaussian filter with a cutoff

frequency minimizing the distortion of sharply rising Ca^{2+} transients. In most cases, we used a 4-pole Butterworth filter with a cutoff frequency equal to 0.2 times the frame rate. We then filtered traces using an iterative procedure to suppress noise but preserve fast Ca^{2+} transients as explained in **Supplementary Figure 3**. We then deconvolved traces linearly by inverse filtering using a kernel $y = \exp(-t/\tau_{decay})$, truncated at $t = 2\tau_{decay}$, where t is time (**Supplementary Fig. 1**). Procedures for filtering and deconvolution procedures were written in Matlab (TheMathWorks).

Note: Supplementary information is available on the Nature Methods website.

ACKNOWLEDGMENTS

We thank W. Denk, T. Euler, J. Kerr, G. Laurent, H. Riecke, P.H. Seeburg and members of the Friedrich laboratory for support, helpful discussions, and/or comments on the manuscript. This work was supported by the Max Planck-Society, the Deutsche Forschungsgemeinschaft (DFG; SFB 488), and a fellowship from the Boehringer Ingelheim Fonds to E.Y.

COMPETING INTERESTS STATEMENT

The authors declare that they have no competing financial interests.

Published online at http://www.nature.com/naturemethods/
Reprints and permissions information is available online at http://npg.nature.com/reprintsandpermissions/

1. Grinvald, A., Frostig, R.D., Lieke, E. & Hildesheim, R. Optical imaging of neuronal activity. *Physiol. Rev.* **68**, 1285–1366 (1988).
2. Zochowski, M. *et al.* Imaging membrane potential with voltage-sensitive dyes. *Biol. Bull.* **198**, 1–21 (2000).
3. Logothetis, N.K. & Pfeuffer, J. On the nature of the BOLD fMRI contrast mechanism. *Magn. Reson. Imaging* **22**, 1517–1531 (2004).
4. Denk, W., Strickler, J.H. & Webb, W.W. Two-photon laser scanning fluorescence microscopy. *Science* **248**, 73–76 (1990).
5. Helmchen, F. & Denk, W. Deep tissue two-photon microscopy. *Nat Methods* **2**, 932–940 (2005).
6. Stosiek, C., Garaschuk, O., Holthoff, K. & Konnerth, A. In vivo two-photon calcium imaging of neuronal networks. *Proc. Natl. Acad. Sci. USA* **100**, 7319–7324 (2003).
7. Brustein, E., Marandi, N., Kovalchuk, Y., Drapeau, P. & Konnerth, A. "In vivo" monitoring of neuronal network activity in zebrafish by two-photon Ca^{2+} imaging. *Pflugers Arch.* **446**, 766–773 (2003).
8. Ohki, K., Chung, S., Ch'ng, Y.H., Kara, P. & Reid, R.C. Functional imaging with cellular resolution reveals precise micro-architecture in visual cortex. *Nature* **433**, 597–603 (2005).
9. Li, J. *et al.* Early development of functional spatial maps in the zebrafish olfactory bulb. *J. Neurosci.* **25**, 5784–5795 (2005).
10. Sullivan, M.R., Nimmerjahn, A., Sarkisov, D.V., Helmchen, F. & Wang, S.S. In vivo calcium imaging of circuit activity in cerebellar cortex. *J. Neurophysiol.* **94**, 1636–1644 (2005).
11. Kerr, J.N., Greenberg, D. & Helmchen, F. Imaging input and output of neocortical networks in vivo. *Proc. Natl Acad. Sci. USA* **102**, 14063–14068 (2005).
12. Helmchen, F., Imoto, K. & Sakmann, B. Ca^{2+} buffering and action potential-evoked Ca^{2+} signaling in dendrites of pyramidal neurons. *Biophys. J.* **70**, 1069–1081 (1996).
13. Laurent, G. Olfactory network dynamics and the coding of multidimensional signals. *Nat. Rev. Neurosci.* **3**, 884–895 (2002).
14. Shipley, M.T. & Ennis, M. Functional organization of olfactory system. *J. Neurobiol.* **30**, 123–176 (1996).
15. Zerucha, T. *et al.* A highly conserved enhancer in the Dlx5/Dlx6 intergenic region is the site of cross-regulatory interactions between Dlx genes in the embryonic forebrain. *J. Neurosci.* **20**, 709–721 (2000).
16. Higashijima, S., Masino, M.A., Mandel, G. & Fetcho, J.R. Imaging neuronal activity during zebrafish behavior with a genetically encoded calcium indicator. *J. Neurophysiol.* **90**, 3986–3997 (2003).
17. Friedrich, R.W. & Laurent, G. Dynamic optimization of odor representations in the olfactory bulb by slow temporal patterning of mitral cell activity. *Science* **291**, 889–894 (2001).
18. Pinault, D. A novel single-cell staining procedure performed in vivo under electrophysiological control: morpho-functional features of juxtacellularly labeled thalamic cells and other central neurons with biocytin or Neurobiotin. *J. Neurosci. Methods* **65**, 113–136 (1996).
19. Friedrich, R.W. & Korsching, S.I. Combinatorial and chemotopic odorant coding in the zebrafish olfactory bulb visualized by optical imaging. *Neuron* **18**, 737–752 (1997).
20. Friedrich, R.W. & Laurent, G. Dynamics of olfactory bulb input and output activity during odor stimulation in zebrafish. *J. Neurophysiol.* **91**, 2658–2669 (2004).
21. Friedrich, R.W., Habermann, C.J. & Laurent, G. Multiplexing using synchrony in the zebrafish olfactory bulb. *Nat. Neurosci.* **7**, 862–871 (2004).
22. Miesenbock, G. & Kevrekidis, I.G. Optical imaging and control of genetically designated neurons in functioning circuits. *Annu. Rev. Neurosci.* **28**, 533–563 (2005).
23. MacLean, J.N., Watson, B.O., Aaron, G.B. & Yuste, R. Internal dynamics determine the cortical response to thalamic stimulation. *Neuron* **48**, 811–823 (2005).
24. Kay, L.M. & Laurent, G. Odor- and context-dependent modulation of mitral cell activity in behaving rats. *Nat. Neurosci.* **2**, 1003–1009 (1999).
25. Chafee, M.V. & Goldman-Rakic, P.S. Matching patterns of activity in primate prefrontal area 8a and parietal area 7ip neurons during a spatial working memory task. *J. Neurophysiol.* **79**, 2919–2940 (1998).
26. Steriade, M., Timofeev, I. & Grenier, F. Natural waking and sleep states: a view from inside neocortical neurons. *J. Neurophysiol.* **85**, 1969–1985 (2001).
27. Wilson, R.I., Turner, G.C. & Laurent, G. Transformation of olfactory representations in the *Drosophila* antennal lobe. *Science* **303**, 366–370 (2004).
28. Singer, W. Neuronal synchrony: a versatile code for the definition of relations? *Neuron* **24**, 49–65 (1999).
29. Wang, J.W., Wong, A.M., Flores, J., Vosshall, L.B. & Axel, R. Two-photon calcium imaging reveals an odor-evoked map of activity in the fly brain. *Cell* **112**, 271–282 (2003).
30. Sachse, S. & Galizia, C.G. The coding of odour-intensity in the honeybee antennal lobe: local computation optimizes odour representation. *Eur. J. Neurosci.* **18**, 2119–2132 (2003).